Libowitzky, E., Beran, A., Wieczorek, A. K., Wirth, R. (2012): On the presence of a hydrous component in a gemstone variety of intermediate olivine-type triphylite-lithiophilite, Li(Fe, Mn)PO4. - Mineralogy and Petrology, 105, 1-2, 31-39

DOI: 10.1007/s00710-012-0195-9

On the presence of a hydrous component in a gemstone variety of intermediate olivine-type triphylite-lithiophilite, $Li(Fe,Mn)PO_4$

Eugen Libowitzky · Anton Beran · Arkadiusz K. Wieczorek · Richard Wirth

Abstract A single-crystal gemstone of intermediate olivine-type triphylite-lithiophilite with the composition $Li(Fe_{0.56}Mn_{0.42})P_{1.02}O_4$ was investigated by vibrational spectroscopy and electron microscopy techniques. Though gem-quality, the crystal reveals lamellar, platy inclusions parallel to (100) with a length of up to > 10 μm and a thickness of up to 1-2 μm. These were identified as sarcopside, $(Fe,Mn)_3(PO_4)_2$, yielding a higher Fe:Mn ratio than the host triphylite. Polarised infrared spectra of oriented triphylite sections show a weak, pleochroic band in the O-H stretching region that is centred at ~ 3444 cm^{-1}. Its integrated total absorbance corresponds to a hydrogen content of only 3.7 wt.ppm H_2O. Using peak-fitting techniques the band is decomposed into three component bands at ~ 3419, 3444, and 3474 cm^{-1} which are least intense in the [010] spectra and which show stronger absorptions in the [001] and [100] directions. Thus, O-H vectors almost parallel to the (010) plane, pointing closer to the *a* or to the *c* axes are assumed. Three ways of hydrogen incorporation are in agreement with this observation: (a) hydrous species at the oriented interfaces between triphylite host and sarcopside lamellae, (b) hydrogen from submicroscopic inclusions of hydrous phosphate minerals such as phosphoferrite-reddingite, $(Fe,Mn)_3(PO_4)_2 \cdot 3H_2O$, (c) hydrous point defects in the structure of triphylite and/or sarcopside, which are possible under the assumption of vacancies at the Li (*M*1) and/or P sites.

Introduction

Minerals of the triphylite-lithiophilite series, $Li(Fe,Mn)PO_4$ occur in evolved granitic pegmatites that are enriched in both lithium and phosphorus and are often altered to a wide variety of secondary hydrous phosphate minerals (Nriagu 1984; Vignola et al. 2011). Triphylite has a definite technical interest in view of its application as a storage cathode for rechargeable lithium batteries (Padhi et al. 1997; Andersson et al. 2000; Prosini et al. 2001; Yamada et al. 2001; Yang et al. 2002; Fehr et al. 2007). Knowledge on the presence of hydrous phases in this rather uncommon mineral may be important for the design of lithium-phosphate storage cathodes.

Triphylite group minerals are isostructural with olivine. Recham et al. (2008) have shown that the dual substitution of Li^{1+} for Fe^{2+} and of P^{5+} for Si^{4+} leads to a complete Fe_2SiO_4-$LiFePO_4$ solid solution series. Temperature-dependent Fe^{2+} Mössbauer parameters of triphylite have been recently reported by Van Alboom et al. (2011). Great interest has been devoted to the modes of OH defect incorporation in natural and annealed Mg-rich (silicate) olivines, especially from kimberlitic xenoliths (Beran and Libowitzky 2006; Keppler and Bolfan-Casanova 2006; Mosenfelder et al. 2006; Gose et al. 2010). OH defects have also been reported in the non-silicate olivine-type minerals chrysoberyl, Al_2BeO_4, and sinhalite, $MgAlBO_4$ (Bauerhansl and Beran 1997). However, comparatively few studies exist on the 'water' content of nominally anhydrous non-silicate mineral phases. In general, the presence of a hydrous phase is often controlled by compositional factors but may also vary as a function of the geological environment.

Infrared (IR) spectroscopy provides an extremely sensitive method for detecting trace amounts of hydrogen bound to oxygen atoms, thus forming OH or H_2O defects in the structures of various nominally anhydrous minerals (Johnson 2006; Libowitzky and Beran 2006; Rossman 2006). By using polarised radiation, the pleochroic scheme of the OH absorption bands provides information on the orientation of the hydrous phases (Libowitzky and Rossman 1996), the wavenumber of an O-H stretching band suggests a certain hydrogen bond length *d*(O-H···O) (e.g. Libowitzky 1999), and the intensity of OH absorption bands provides information on concentration (e.g. Libowitzky and Rossman 1997). Nevertheless, by discussing OH absorption spectra of nominally anhydrous minerals, the presence and the oriented intergrowth of microscopic to submicroscopic hydrous mineral inclusions have to be considered. Based on this method it is the principal aim of the present paper to characterise the absorption properties of triphylite in the OH stretching vibrational region and to discuss plausible models for the incorporation of hydrous phases into the close-packed structure of this phospho-olivine mineral with potential technical implication.

Experimental

Sample description and sample preparation

A cut, single-crystal gemstone of intermediate triphylite-lithiophilite from an unknown locality in Brazil, with exceptional optical quality, and with an approximate size of about 0.3 x 0.3 x 0.6 cm, was used for the present investigation. Unfortunately, there exist some ten

Brazilian triphylite occurrences in the states Minas Gerais, Paraíba, and Rio Grande do Norte (www.mindat.org). However, due to hints on bad crystal quality and diverging chemistry, most localities can be excluded. There remain only two probable phosphate pegmatites, i.e. the Cigana claim (Jocão claim), Minas Gerais (no composition available; hints on "gem material"), and the Serra Branca pegmatite, Paraíba. The latter occurrence appears most compelling, as the triphylite composition with Fe/(Fe+Mn) = 0.55 and the lattice parameters (*Pmnb* setting) *a* = 6.052 and 6.048 Å, *b* = 10.391 and 10.337 Å, *c* = 4.715 and 4.704 Å (sample P100 from Fransolet et al. 1984 and Langer et al. 2006) are almost identical to those of the present specimen (see below).

From ten energy-dispersive X-ray spectrometry (EDS) analyses (for experimental details see below) the formula $Li(Fe_{0.56}Mn_{0.42})P_{1.02}O_4$ was obtained. As Li cannot be analysed with EDS, it was assumed as 1.00 atoms per formula unit (*apfu*). Analysis of Li by other methods such as (i) atomic absorption spectrometry (AAS) or (ii) laser-induced breakdown spectroscopy (LIBS) was declined as these techniques are either (i) a destructive bulk method or (ii) rather inaccurate (± 20 % rel.) with low lateral resolution (6-8 µm; Fabre et al. 2002).

The crystal piece was oriented by X-ray single-crystal diffraction using a Nonius Kappa CCD four-circle diffractometer. In two sequences of preparation, the gemstone was cut with a low-speed diamond wheel saw parallel to (100) and (010). Subsequently, the crystal was attached with the existing faces on a sample grinder and cut and polished on both opposite sides to a final thickness of 0.2 cm in both directions, thus forming a pseudo-tetragonal prism. In addition, following the same preparation procedure, a 0.1 cm thick crystal plate, cut and polished parallel to (001) was prepared.

The used indices refer to the lattice parameters *a* = 4.705(5), *b* = 10.381(10) and *c* = 6.041(6) Å, space group *Pbnm*, obtained during the X-ray single-crystal inspection above (due to the large crystal size and the quick procedure the estimated standard deviation of the lattice parameters is not better than 0.1 % relative). They are in good agreement with the refinement data given by Losey et al. (2004) for an intermediate ($Fe_{0.50}Mn_{0.50}$) crystal (sample Trip50) of the triphylite-lithiophilite solid solution series (see also Padhi et al. 1997; Yang et al. 2002). Even better, using linear regression of lattice parameters between Trip06 and Trip79 (including/excluding the Mg-rich sample Trip89) from Losey et al. (2004), X_{Fe} values of 0.54 - 0.58 are obtained, confirming the EDS data above.

FTIR and Raman spectroscopy, SEM, TEM, and EDS analyses

Polarised single-crystal spectra were recorded from 5000 to 2000 cm^{-1} with a Bruker IFS 66v/S Fourier-transform infrared (FTIR) spectrometer, which was equipped with a glo(w)bar light source, a liquid nitrogen-cooled MCT detector and a KRS-5 wire-grid polariser. Background and sample spectra were obtained from 128 scans with a spectral resolution of 2 cm^{-1}. The oriented crystal was mounted on a brass sample holder with a circular aperture of 500 μm in diameter. In addition, data were also checked with a Bruker TENSOR27 FTIR spectrometer using an identical setup, except for a DLATGS detector, 4000-2500 cm^{-1} range, 4 cm^{-1} spectral resolution, and a 1.5 mm aperture. (By this means, an ambiguous spectral feature at ~ 3250 cm^{-1} could be assigned to traces of condensed humidity at the cold MCT detector window.) After background correction the spectra were decomposed into single Voigt- (Gaussian- and Lorentzian-) shaped component bands, using the program PeakFit 4.12 (Seasolve Software Inc.).

Raman spectra were acquired by using an edge filter-based confocal Renishaw RM1000 micro-Raman spectrometer in the spectral range from <100 to 4000 cm^{-1}. The 488 nm excitation line of a 20 mW Ar+ laser and the 632.8 nm excitation line of a 20 mW HeNe laser were focused with a 50x/0.75 objective on the sample surface. Spectra were calibrated with the Rayleigh line and a Si standard. Minimum spatial resolution was ~ 2-3 μm, the spectral resolution (apparatus function) was ~ 4 cm^{-1}.

The crystal was inspected and analysed by a Jeol JSM-6400 scanning electron microscope (SEM), operated at 10 kV (for imaging and qualitative EDS micro-analyses) or 20 kV (for quantitative EDS analyses), equipped with a Link EDS system. Pure elemental standards, averaging of ten point analyses, and correction by the ZAF procedure were applied for the quantitative analyses of the triphylite sample (see above).

A FEI Tecnai G2 F20 X-Twin operating at 200 kV with field emission gun electron source was utilized for the transmission electron microscopy (TEM) studies. An attached EDAX EDS system with ultrathin window was used for chemical analyses and mapping. Oriented TEM sample preparation was carried out in advance by using the focused ion beam (FIB) technique (Ga-ion source, 30 kV acceleration voltage) on a FEI FIB 200 TEM (Wirth 2004; 2009).

Results

Optical inspection

Under the optical polarising microscope, in transmitted light the (100) crystal section shows a distinct pleochroism with an orange-brown colour parallel to [001] and a light greenish-grey colour parallel to [010]. In the (010) section, a light brownish-grey colour occurs parallel to [100]. The slightly different colours parallel to [100] and [010] are also discernable in the (001) section and confirm the weak pleochroism (Langer et al. 2006). In comparison to the (100) section, the (010) section shows a slightly turbid appearance resulting from rows of micro-scale lamellae with a strongly preferred orientation parallel to [001], reminding of a lamellar exsolution texture. Optical examination of the (001) crystal plate reveals a similar diffuse pattern with rows of spindles, giving evidence for the presence of platelet-shaped phases oriented parallel to (100). The size of these features ranges in the micrometer scale, i.e. > 10 μm length and < 1-2 μm width (Fig. 1). In the centre of some spindles a dark spot (micro-inclusion) is sometimes revealed. In contrast to the perfect extinction on the (100) section, the (010) and (001) sections show a dark blue interference colour under crossed polarisers. In polarised reflected light, the polished (100), (010) and (001) sections show a weak but distinct reflection pleochroism. By observing the (010) and (001) polished sections under crossed polarisers, internal reflections also reveal the described faint exsolution texture.

IR spectra of triphylite

The OH absorption feature of triphylite is characterised by a relatively broad absorption band at ~ 3444 cm^{-1}. The IR spectra are complicated by a steep and curved background slope (inset of Fig. 2) resulting from the influence of the strong PO_4 stretching fundamentals ($\nu_{1,3}$ ~ 900-1100 cm^{-1}) and their first overtone vibrations ($2\nu_{1,3}$ ~ 1800-2200 cm^{-1}). Moreover, several weak and broad features between 2800 and 3300 cm^{-1} corrupt the spectra. These were assigned to the second overtones of PO_4 stretching vibrations ($3\nu_{1,3}$ ~ 2700-3300 cm^{-1}) and artefacts from condensation of humidity at the cold detector window (see above), and thus were included in the background correction. Polarised OH absorption spectra measured on (100) and (010) faces with the electric vector ***E*** of the polarised IR radiation vibrating parallel to [100], [010] and [001] are shown in Fig. 2a-c. On the basis of clearly observable band maxima and shoulders of the spectra measured parallel to [100] and [010], the decomposition and fit ($r^2 > 0.99$) of all absorption features requires a minimum of three component bands centred at 3470 - 3474, 3441 - 3444, and 3419 - 3424 cm^{-1}. (The data variability results from the fact that the component peaks were absolutely unconstrained in position, height, and width during the refinement of each polarised spectrum.) Band decomposition of the most intense

spectrum measured parallel to [001] reveals band maxima at 3474, 3444 and 3419 cm^{-1}. The dominating band at 3444 cm^{-1} shows maximum absorption, when the vector of the polarised radiation vibrates parallel to [001]. Only weak absorptions are present parallel to [100] and [010], regardless if peak heights or areas are compared (Fig. 2). Weak absorption components with comparable intensities parallel to [100] and [001] and subordinate absorption parallel to [010] are evident for the 3474 cm^{-1} band. The 3419 cm^{-1} band has its weakest component also parallel to [010].

IR spectroscopic determination of the 'water' concentration

The linear absorption coefficient of an absorption band is defined as $\alpha = A/t$, where A is the linear absorbance, log (I_0/I), and t is the thickness of the crystal measured in cm (here t = 0.2 cm). The integrated absorbance values A_i (cm^{-1}) measured parallel to [100], [010] and [001] were summed up to get the total integrated absorbance value $A_{i\ total}$ (= 11.0 cm^{-1}) which was used for the calculation of the integrated absorption coefficient α_i (cm^{-2}), according to the relation $\alpha_i = A_{i\ total}/t$ (= 55.0 cm^{-2}). As expressed by Beer-Lambert's law, α_i is directly related by the integrated molar absorption coefficient ε_i ($l*mol^{-1}*cm^{-2}$) to the concentration c ($mol*l^{-1}$). The water content in wt% is calculated using the relationship $c_{H2O} = (1.8/D)(\alpha_i/\varepsilon_i)$, where D is the density of the mineral (using 3.5 g/cm^3 for intermediate triphylite-lithiophilite) (Beran et al. 1993; Libowitzky and Beran 2004). The ε_i value deduced from the general calibration curve given by Libowitzky and Rossman (1997) amounts to 77200 $l*mol^{-1}*cm^{-2}$. Thus, the resulting 'water' concentration is 3.7 wt.ppm H_2O.

TEM and RAMAN study

Figure 3a depicts a TEM image in bright-field (BF) mode of a FIB section of the triphylite sample with one of the lamellae described above. The strictly parallel orientation of lamellae that was already observed under the optical microscope is confirmed. Moreover, each spindle shows an alternating dark and bright contrast pattern which is caused by polysynthetic twinning. An EDS line scan (P-K_α, Fe-K_α, Mn-K_α) across the individual twins normal to the twin boundaries did not show any change in chemical composition of the lamellae, which suggests the bright and dark contrast pattern to be not an effect of two different intergrown phases. As part of the TEM study, the chemical composition of the included lamellar phase was determined by EDS as a phosphate mineral with significantly higher Fe (38.5 at%),

almost unchanged Mn (19.2 at%) and lower P contents (42.3 at%) than in the surrounding triphylite (27.8 at% Fe, 21.3 at% Mn, 50.9 at% P). The different chemical compositions of the twinned lamellae and the host phase cause strain contrast (white arrows in Fig. 3a), which is a result of lattice mismatch between lamella and matrix. Elemental distribution maps with high spatial resolution that depict enrichment of Fe and depletion of P are shown in Fig. 3b,c. From high-resolution imaging and resulting diffraction pattern of matrix plus lamellae (Fig. 4a,b) the following orientation relationship between matrix and lamellae was observed: $(010)_{tr}$ // $(100)_{sar}$; $(100)_{tr}$ // $(010)_{sar}$; $(110)_{tr}$ // $(110)_{sar}$.

The micro-Raman spectra (Fig. 5) obtained from the exsolution lamellae (pure spectra could only be obtained after subtraction of the triphylite host spectra), and their comparison with reference spectra from the RRUFF database (Downs 2006), clearly prove the presence of sarcopside, $(Fe,Mn)_3(PO_4)_2$ as the dominating mineral phase, which is commonly observed in the form of exsolutions in triphylite (Smeds et al. 1998, Hatert et al. 2007, Roda-Robles et al. 2011), and whose composition is also in perfect agreement with the analytical data obtained by TEM-EDS (see above). Moreover, the observed polysynthetic twinning in the TEM image (Fig. 3a) is indeed a characteristic feature of sarcopside (Hurlbut 1965), and its crystal structure and lattice parameters are closely related to those of triphylite, thus facilitating oriented mutual intergrowth (see below). However, according to its stoichiometry sarcopside is an anhydrous phosphate mineral and thus cannot be invoked as source of a hydrous component indicated by the OH absorption bands in the IR spectra of triphylite. Nevertheless, incorporation of hydrogen in the form of defects is well possible for both host triphylite and sarcopside lamellae (see discussion below).

Repeated acquisition of micro-Raman spectra and qualitative SEM EDS analyses of the central micro-inclusions in the lamellae (see above and Fig. 1) eventually identified two hydrous minerals, i.e., muscovite (OH stretching band at ~ 3630 cm^{-1}; K, Al, Si in EDS) and apatite (OH stretching band at ~ 3570 cm^{-1}; Ca, P in EDS).

Discussion

The structure of the triphylite-lithiophilite series, $Li(Fe,Mn)PO_4$, has the olivine topology (Losey et al. 2004). One formula unit contains two crystallographically different *M* sites, i.e., *M*1 on a centre of symmetry, and *M*2 in a mirror plane. P is also placed in the mirror plane. Two of the three oxygen positions, O1 and O2, are located in a mirror plane, while the third, O3, occupies a general position (Fig. 6). All oxygen atoms are coordinated by three *M* cations

and one P atom in the form of a distorted tetrahedron, i.e., O3: 2 x *M*2 , *M*1, P; O2 and O1: 2 x *M*1, *M*2, P. The complete ordering of cations with Li at the *M*1 site and (Fe,Mn) at the *M*2 site is in contrast to the majority of olivine-structure phases, in which there is extensive disorder among the octahedrally coordinated cations at the *M* sites (Losey et al. 2004).

The exsolution lamellae observed in the present study of intermediate gem-quality triphylite-lithiophilite, have been clearly identified as sarcopside (see above). The structure of sarcopside, $V(Fe,Mn)(Fe,Mn)_2(PO_4)_2$ can be easily derived from the structure of triphylite $Li_2(Fe,Mn)_2(PO_4)_2$ by the presence of ordered vacancies (*V*) and Fe/Mn atoms at the Li (*M*1) sites (Moore, 1984). As a consequence, the lattice parameters of triphylite (a = 4.71, b = 10.38, c = 6.04 Å) are in close agreement with those of monoclinic (pseudo-orthorhombic) sarcopside (a = 10.44, b = 4.77, c = 6.03 Å, β = 90°; Moore 1972) which implies that the (010) plane of sarcopside is oriented parallel to the (100) plane of triphylite. This is also demonstrated from FFT from high-resolution TEM images (Fig. 4b).

The observation of a group of weak O-H stretching bands (equivalent to only 3.7 wt-ppm H_2O) at about 3419, 3444, and 3474 cm^{-1} in the polarised IR spectra of triphylite, which show different band intensities in different crystal orientations (pleochroism with maximum absorption parallel to [001]), indicates that the hydrous species (OH^-/H_2O) have a certain structural relation to the sample. Three possibilities of hydrogen incorporation can be considered, which are in agreement with this observation: (a) hydrous species at the interface between triphylite host and oriented sarcopside lamellae, (b) hydrous species resulting from the incorporation/exsolution of sub-microscopic hydrous mineral phases in the triphylite host, (c) hydrous point defects in the structure of triphylite and/or sarcopside.

(a) The presence of oriented hydrous species at the interface between triphylite host and sarcopside lamellae appears reasonable, because these extremely thin and flat inclusions have a certain structural relation and orientation to each other (see above) and thus provide a well defined environment for structurally aligned water and/or hydroxyl groups in the distorted interface region (strain contrast at the interface, Fig. 3a). Although the general distortion of the interface region is assumed low due to similar lattice parameters of both phases (see above), local distortions in the form of vacant and Fe/Mn-substituted Li sites and resulting local strain may provide suitable sites for structurally constrained hydrogen incorporation. As a further argument, the wavenumbers of the IR absorption bands in triphylite are well comparable to the frequently observed broad 3400 cm^{-1} absorption band caused by moisture (water molecules) adsorbed to grain boundaries of KBr powder pellets or

to the surfaces of IR-transparent lenses and windows crafted from KBr. However, in contrast to the present study, the band in KBr is isotropic due to the cubic symmetry (optically isotropic) and the random orientation of grain boundaries in KBr pellets.

(b) Potential hydrous micro-inclusions in triphylite were predominantly searched for in the RRUFF data base (Downs 2006). The use of compositional constraints, i.e. presence of Fe or Mn, P, O, H, (Li), resulted in approximately 20 hints, which were later expanded by IR/Raman spectra of further compounds from the internet and from spectral data books.

Two hydrous phosphate minerals appear as ideal candidates, i.e., phosphoferrite, $(Fe,Mn)_3(PO_4)_2 \cdot 3H_2O$, and reddingite, $(Mn,Fe)_3(PO_4)_2 \cdot 3H_2O$, both representing the end-members of a complete solid solution series. Their chemical composition corresponds exactly to that of sarcopside + $3H_2O$. They are well known to occur as hydrothermal alteration products of triphylite (Moore 1984), and the Raman spectra of both minerals, available from the RRUFF data base (Downs 2006), are characterised by a strong O-H stretching band at 3443 cm^{-1} and a broad band/shoulder on the low-energy side at ~3200 cm^{-1}. The spectra were also confirmed by own independent Raman and IR measurements (KBr pellets and ATR technique) of two reference samples. The former band position is in perfect agreement with the observed band at 3444 cm^{-1}, dominating the unpolarised IR spectrum in the OH stretching vibrational region of triphylite and its polarised spectrum measured parallel to [001]. However, on the one hand the component bands at 3419/3474 cm^{-1} in the IR spectra of triphylite remain still unassigned, and on the other hand the broad band/shoulder of phosphoferrite-reddingite at ~ 3200 cm^{-1} is not observed undoubtedly (due to the complicated background shape - see above) in the triphylite spectra. However, considering the water content of stoichiometric phosphoferrite which amounts to ~ 13 wt.% H_2O, the observed water content of triphylite (3.7 wt.ppm H_2O) requires an extremely low concentration of this hydrous mineral phase. Despite similarities in the lattice parameters ($a/2$ = 4.73, b = 10.02, c = 8.67 Å for phosphoferrite; Moore and Araki 1976) triphylite and phosphoferrite have differing structural features, thus rendering a structurally controlled oriented intergrowth unlikely.

The presence of the structurally related oxidised phosphate phase kryzhanovskite, $Fe^{3+}{}_3(OH)_3(PO_4)_3$, frequently occurring together with phosphoferrite, can be excluded due to the fact that this mineral is characterised by a Raman spectrum with an OH stretching band at 3580 cm^{-1} which is not observed in the present triphylite sample. In a similar way, the oxidised phase tavorite, $LiFe^{3+}(OH)(PO_4)$, with an OH stretching band at 3269 cm^{-1} can be

excluded (RRUFF database; Downs 2006). However, according to electron energy-loss spectroscopy (EELS) data from the TEM investigation, the presence of minor amounts of Fe^{3+} in triphylite can be assumed. Charge compensation is easy to provide by the incorporation of a ferrisicklerite component, $(Li,V_{Li})(Fe^{3+},Mn)(PO_4)$ containing vacant Li sites (V_{Li}). In a similar way, the presence of minor Mn^{3+} contents in the observed sarcopside lamellae is also suggested by EELS. Nevertheless, a possible presence of heterosite, $Fe^{3+}(PO_4)$, cannot be confirmed in the triphylite sample, neither in traces by IR spectroscopy (no OH signal) nor in minor amounts by Raman spectroscopy (different Raman fingerprint).

The bands at 3419 and 3474 cm^{-1}, not explained by the spectrum of phosphoferrite, require the presence of an additional hydrous phase. Candidates from the RRUFF data base (Downs 2006) with the most suitable Raman O-H stretching bands are strunzite, $MnFe^{3+}_2[(OH)(PO_4)]_2 \cdot 6H_2O$ (two bands at ~ 3410 and 3510 cm^{-1}) - ferrostrunzite, $Fe^{2+}Fe^{3+}_2[(OH)(PO_4)]_2 \cdot 6H_2O$ (two bands at ~ 3370 and 3470 cm^{-1}). However, the spectral fit is only moderate. The frequent solid-solution series wolfeite-triploidite, $(Fe,Mn)_2(OH)(PO_4)$-$(Mn,Fe)_2(OH)(PO_4)$ is also unlikely, as the OH stretching bands occur at 3518 (Raman) or 3496 cm^{-1} (IR-ATR) for wolfeite (RRUFF database; Downs 2006) and the Mn-rich endmember is expected to show even higher values due to the larger lattice parameters.

(c) Considering the presence of OH groups in the form of structural point defects, the observed pleochroic O-H stretching bands can be assigned to OH point defects similar to those frequently observed in the structure of olivines from different occurrences (Beran and Libowitzky, 2006). Thus, a geometrically and crystal chemically plausible model for an OH point defect position in triphylite (and due to its similar structure also in sarcopside) can be derived under the assumption of vacancies in the cation sublattice. In addition, using the d - ν correlation diagram of Libowitzky (1999), relating O-H···O distances and stretching wavenumbers (see also Novak 1974), an O-H···O distance of about 2.80 - 2.85 Å is expected for the bands at 3419, 3444, 3474 cm^{-1}.

The pleochroism of the absorption bands with a generally very weak component parallel to [010], requires a preferred orientation of the O-H dipoles approximately in the (010) plane. Slight deviations from (010) are inferred from the weak components (instead of absence of bands) parallel to [010]. In contrast to the 3475 cm^{-1} band with a stronger component parallel to [100] and a slightly weaker component parallel to [001], the bands at 3419 and 3444 cm^{-1} have their strongest absorption parallel to [001] and a weaker component

parallel to [100] (Fig. 2). Thus, the former band is oriented closer to the [100] direction, the latter two are closer to [001].

Assuming vacancies at the Li (*M*1) sites (Fig. 6), OH defects pointing roughly parallel to the O1-*M*1 vector, would be consistent with the observed pleochroic behaviour of the bands. This direction coincides perfectly with a line approximately perpendicular to the plane of the three "remaining" coordinating cations around O1, repelling the H atom by electrostatic Coulomb forces. Slight deviations from this line are caused by different charges of the different coordinating cations. For pure triphylite this OH point defect is coordinated by one Li (*M*1), one Fe^{2+} (*M*2) and one P, where O1 acts as donor oxygen (Fig. 6). This model is based on the plausible assumption of a vacant Li (*M*1) site as it is also found in the related structures of sarcopside and ferrisicklerite. Considering local distortions, the O1···O3 distance of 2.93 Å is in fair agreement with the expected H bond length (see above), thus making the O3 oxygen atom, coordinating the vacant Li site, a favourable acceptor oxygen of a strongly kinked O-H···O bond. The O2 atom at an O1···O2 distance of 3.08 Å may also act as an additional H bond acceptor, thus forming an asymmetric bifurcated H bond.

Another OH defect is proposed under the assumption of a vacant P site, comparable to the "hydrogarnet" defect in silicate minerals (Libowitzky and Beran 2006). Thus O3 may act as donor oxygen for an OH group pointing roughly along the O3 - O3 line close to the centre of the vacant PO_4 tetrahedron (Fig. 6). The O-H vector is again perpendicular to the plane of the three remaining *M* cations, as required by Coulomb repulsion. The intra-tetrahedral O3···O3 distance amounts to 2.45 Å which is in severe disagreement with the expected H bond distance of ca. 2.80 - 2.85 Å. However, it must be emphasized that due to the vacant centre of the tetrahedron its size is expanded by ca. 20% (in analogy to hydrogrossular). As a consequence, the relaxed O3···O3 distance is assumed as ~ 2.94 Å which is in fair agreement with the expected O-H···O distance.

Though only two different OH point defect types are considered above, a wide variety of defects and related absorption bands with slightly different wavenumbers and pleochroic behaviour emerge from substitution at the three coordinating cation sites connected to the O-H groups. Thus, in case of the intermediate triphylite-lithiophilite sample of the present study *M*2 is approximately equally occupied by Fe^{2+} and Mn^{2+}. Fe^{3+} and Mn^{3+} must be also considered to provide charge balance for vacant Li sites (see ferrisicklerite above) and/or for a vacant P site. In case of defects in the sarcopside lamellae, Li at *M*1 is replaced by vacancies and by Fe/Mn atoms, giving rise to additional defect environment and related O-H stretching bands.

Comparing the OH defect incorporation in triphylite with that in isostructural olivine, a generally different preference of incorporation modes is evident. In contrast to triphylite, most of the OH absorption bands in olivine occur at higher wavenumbers and are strongly polarised parallel to [100]. However, few exceptions exist in olivines where rarely occurring lower-energetic absorption bands are polarised parallel to [001] (Beran and Putnis 1983; Lemaire et al. 2004). A common feature of the OH defect incorporation modes in phospho- and silicate olivines is the basic requirement for the presence of vacancies on cation sites. No plausible models are derivable by simply assuming charge imbalances on fully occupied cation sites coordinating the OH defects.

For technical applications in Li batteries, one may speculate whether "OH defect-induced" Li vacancies on *M*1 sites may have an effect on the activation energy for Li diffusion. A change of the activation energy can be expected by the presence of higher-energetic Li-OH bonds, due to the replacement of coordinating oxygen atoms by OH point defects.

Acknowledgements Thanks are due to G. Giester for help with X-ray single-crystal orientation and lattice parameter determination, and to A. Wagner for sample preparation. B. Rieck provided two reference samples of phosphoferrite and reddingite. The comments of two anonymous referees and of journal editor R. Abart helped to improve the manuscript. We appreciate financial support by the European Commission through the program Human Potential-Research Training Network, No. HPRN-CT-2000-0056, "Hydrogen Speciation in Upper Mantle Minerals".

References

Andersson AS, Thomas JO, Kalska B, Häggström L (2000) Thermal stability of $LiFePO_4$-based cathodes. Electrochem Solid-State Letters 3:66-68

Bauerhansl P, Beran A (1997) Trace hydrogen in the olivine-type minerals chrysoberyl, Al_2BeO_4 and sinhalite, $MgAlBO_4$ – a polarized FTIR spectroscopic study. Schweiz Mineral Petrogr Mitt 77:131-136

Beran A, Libowitzky E (2006) Water in natural mantle minerals II: Olivine, garnet and accessory minerals. In: H Keppler, JR Smyth (eds), Water in Nominally Anhydrous Minerals. Rev Mineral Geochem 62:169-191

Beran A. Putnis A (1983) A model of the OH positions in olivine, derived from infrared-spectroscopic investigations. Phys Chem Minerals 9:57-60

Beran A, Langer K, Andrut M (1993) Single crystal infrared spectra in the range of OH fundamentals of paragenetic garnet, omphacite and kyanite in an eclogitic mantle xenolith. Mineral Petrol 48:257-268

Downs RT (2006) The RRUFF Project: an integrated study of the chemistry, crystallography, Raman and infrared spectroscopy of minerals. Program and Abstracts of the 19th General Meeting of the International Mineralogical Association in Kobe, Japan. O03-13

Fabre C, Boiron M-C, Dubessy J, Chabiron A, Charoy B, Crespo TM (2002) Advances in lithium analysis in solids by means of laser-induced breakdown spectroscopy: An exploratory study. Geochim Cosmochim Acta 66:1401-1407

Fehr KT, Hochleitner R, Schmidbauer E, Schneider J (2007) Mineralogy, Mössbauer spectra and electrical conductivity of triphylite $Li(Fe^{2+},Mn^{2+})PO_4$. Phys Chem Minerals 34:485-494

Fransolet A-M, Antenucci D, Speetjens J-M (1984) An X-ray determinative method for the divalent cation ratio in the triphylite-lithiophilite series. Min Mag 48:373-381

Gose J, Schmädicke E, Markowitz M, Beran A (2010) OH point defects in olivine from Pakistan. Mineral Petrol 99:105-111

Hatert F, Roda-Robles E, Keller P, Fontan F, Fransolet A-M (2007) Petrogenetic significance of the triphylite + sarcopside intergrowths in granitic pegmatites: an experimental investigation of the $Li(Fe,Mn)(PO_4)$-$(Fe,Mn)_3(PO_4)_2$ system. Granitic Pegmatites: The State of the Art, Int Symp Book of Abstr 44

Hurlbut CS (1965) Detailed description of sarcopside from East Alstead, New Hampshire. Am Mineral 50:1698-1707

Johnson EA (2006) Water in nominally anhydrous crustal minerals: Speciation, concentration and geologic significance. In: H Keppler, JR Smyth (eds), Water in Nominally Anhydrous Minerals. Rev Mineral Geochem 62:117-154

Keppler H, Bolfan-Casanova N (2006) Thermodynamics of water solubility and partitioning. In: H Keppler, JR Smyth (eds), Water in Nominally Anhydrous Minerals. Rev Mineral Geochem 62:193-230

Langer K, Taran MN, Fransolet A-M (2006) Electronic absorption spectra of phosphate minerals with olivine-type structures: I. Members of the triphylite-lithiophilite series, $^{M1[6]}Li^{M2[6]}(Fe_x^{2+}Mn_{1-x}^{2+})[PO_4]$. Eur J Mineral 18:337-344

Lemaire C, Kohn SC, Brooker RA (2004) The effect of silica activity on the incorporation mechanisms of water in synthetic forsterite: a polarised infrared spectroscopic study. Contrib Mineral Petrol 147:48-57

Libowitzky E (1999) Correlation of O-H stretching frequencies and O-H···O hydrogen bond lengths in minerals. Mh Chem 130:1047-1059

Libowitzky E, Beran A (2004) IR spectroscopic characterisation of hydrous species in minerals. In: A Beran, E Libowitzky (eds), EMU Notes Mineral, Vol 6. Eötvös Univ Press, p 227-279

Libowitzky E, Beran A (2006) The structure of hydrous species in nominally anhydrous minerals: Information from polarized IR spectroscopy. In: H Keppler, JR Smyth (eds), Water in Nominally Anhydrous Minerals. Rev Mineral Geochem 62:29-52

Libowitzky E, Rossman GR (1996) Principles of quantitative absorbance measurements in anisotropic crystals. Phys Chem Minerals 23:319-327

Libowitzky E, Rossman GR (1997) An IR absorption calibration for water in minerals. Am Mineral 82:1111-1115

Losey A, Rakovan J, Hughes JM, Francis CA, Dyar MD (2004) Structural variation in the lithiophilite-triphylite series and other olivine-group structures. Can Mineral 42:1105-1115

Moore PB (1972) Sarcopside: Its atomic arrangement. Am Mineral 57:24-35

Moore PB (1984) Crystallochemical aspects of the phosphate minerals. In: JO Nriagu and PB Moore (eds), Phosphate Minerals. Springer: Berlin, pp.155-170

Moore PB, Araki T (1976) A mixed-valence solid-solution series: Crystal structures of phosphoferrite, $Fe^{II}_3(H_2O)_3[PO_4]_2$, and kryzhanovskite, $Fe^{III}_3(OH)_3[PO_4]_2$. Inorg Chem 15:316-321

Mosenfelder JL, Deligne NI, Asimow PD, Rossman GR (2006) Hydrogen incorporation in olivine from 2-12 GPa. Am Mineral 91:285-294

Novak A (1974) Hydrogen bonding in solids: correlation of spectroscopic and crystallographic data. Struct Bond 18:177-216

Nriagu JO (1984) Phosphate minerals: Their properties and general modes of occurrence. In: JO Nriagu and PB Moore (eds), Phosphate Minerals. Springer: Berlin, pp.1-136

Padhi AK, Nanjundaswamy KS, Goodenough JB (1997) Phospho-olivines as positive-electrode materials for rechargeable lithium batteries. J Electrochem Soc 144:1188-1194

Prosini PP, Zane D, Pasquali M (2001) Improved electrochemical performance of a $LiFePO_4$-based composite cathode. Electrochim Acta 46:3517-3523

Recham N, Casas-Cabanas M, Cabana J, Grey CP, Jumas J-C, Dupont L, Armand M, Tarascon J-M (2008) Formation of a complete solid solution between the triphylite and fayalite olivine structures. Chem Mater 20:6798-6809

Roda-Robles E, Galliski M, Nizamoff J, Simmons W, Keller P, Falster A, Hatert A (2011) Cation partitioning between minerals of the triphylite ± graftonite ± sarcopside association in granitic pegmatites. 5th Int Symp on granitic pegmatites - PEG2011, Abstract book 161-164

Rossman GR (2006) Analytical methods for measuring water in nominally anhydrous minerals. In: H Keppler, JR Smyth (eds), Water in Nominally Anhydrous Minerals. Rev Mineral Geochem 62:1-28

Smeds S-A, Uher P, Černý P, Wise MA, Gustafsson L, Penner P (1998) Graftonite - busite in Sweden: primary phases, products of exsolution, and distribution in zoned populations of granitic pegmatites. Can Mineral 36:377-394

Van Alboom A, De Grave E, Wohlfahrt-Mehrens M (2011) Temperature dependence of the Fe^{2+} Mössbauer parameters in triphylite ($LiFePO_4$). Am Mineral 96:408-416

Vignola P, Diella V, Ferrari ES, Fransolet A-M (2011) Complex mechanisms of alteration in a graftonite + sarcopside + triphylite association from the Luna pegmatite, Piona, Lecco Province, Italy. Can Mineral 49:765-776

Wirth R (2004) A novel technology for advanced application of micro- and nanoanalysis in geosciences and applied mineralogy. Eur J Mineral 16:863-876

Wirth R (2009) Focused Ion Beam (FIB) combined with SEM and TEM: Advanced analytical tools for studies of chemical composition, microstructure and crystal structure in geomaterials on a nanometre scale. Chem Geol 261:217-229

Yamada A, Chung SC, Hinokuma K (2001) Optimized $LiFePO_4$ for lithium battery cathodes. J Electrochem Soc 148:A224-A229

Yang S, Song Y, Zavalij PY, Whittingham MS (2002) Reactivity, stability, and electrochemical behavior of lithium iron phosphates. Electrochem Commun 4:239-244

Figure captions

Fig. 1 Sarcopside lamellae of > 10 μm length and < 1-2 μm width in a slab of triphylite. Sometimes they contain a tiny inclusion in their central part. Optical micrograph in reflected light.

Fig. 2 Polarised, background-corrected FTIR spectra of an oriented single-crystal slab of triphylite, each decomposed into three Voigt-shaped bands at 3470 - 3474, 3441 - 3444, and 3419 - 3424 cm^{-1} measured with the ***E*** vector of the polarised radiation (a) parallel to [100], (b) [010], and (c) [001]. The inset shows an example of a raw spectrum corrupted by a steep and curved background slope from PO_4 stretching fundamentals and overtones as well as condensed humidity.

Fig. 3 TEM investigation of a triphylite FIB section containing lamellar features of ~ 0.5 - 1 μm length and ~ 0.1 μm width. (a) TEM bright-field (BF) image of one lamella showing an alternating dark and bright contrast pattern from polysynthetic twinning. The white arrows point to regions with visible strain contrast at the interface between lamella and host. EDS elemental distribution maps reveal (b) depletion of P, and (c) enrichment of Fe in a lamella compared to the host phase.

Fig. 4 (a) High-resolution TEM lattice fringe image showing the rounded tip of a sarcopside lamella ending in the triphylite matrix. The lattice fringes $(100)_{sarcopside}$ and $(010)_{triphylite}$ are indicated. There is nearly perfect match between the two lattice planes. (b) The calculated diffraction pattern from the HREM image (fast Fourier transform FFT) shows a perfect single- crystal pattern with the triphylite indexed in black and the sarcopside indexed in white.

Fig. 5 Micro-Raman spectra of sarcopside lamellae, triphylite host phase, and reference spectra from the RRUFF database (Downs 2006). Spectra were normalised to max. intensity = 1.0, and each vertically offset by intensity = 1.0. Sarcopside spectra were improved by subtraction of spectral components from the host triphylite.

Fig. 6 The olivine-type crystal structure of triphylite with two proposed OH point defects related to a vacant *M*1 (V_{M1}) and P (V_P) site, respectively. In intermediate triphylite-lithiophilite *M*1 is occupied by Li and *M*2 by Fe and Mn. Solid lines are cation - oxygen bonds within coordination polyhedra, broken lines indicate H···O hydrogen bonds (see text). Blue lines belong to the first coordination sphere of the OH defects; H atoms are plotted in pale blue.

Figure 1

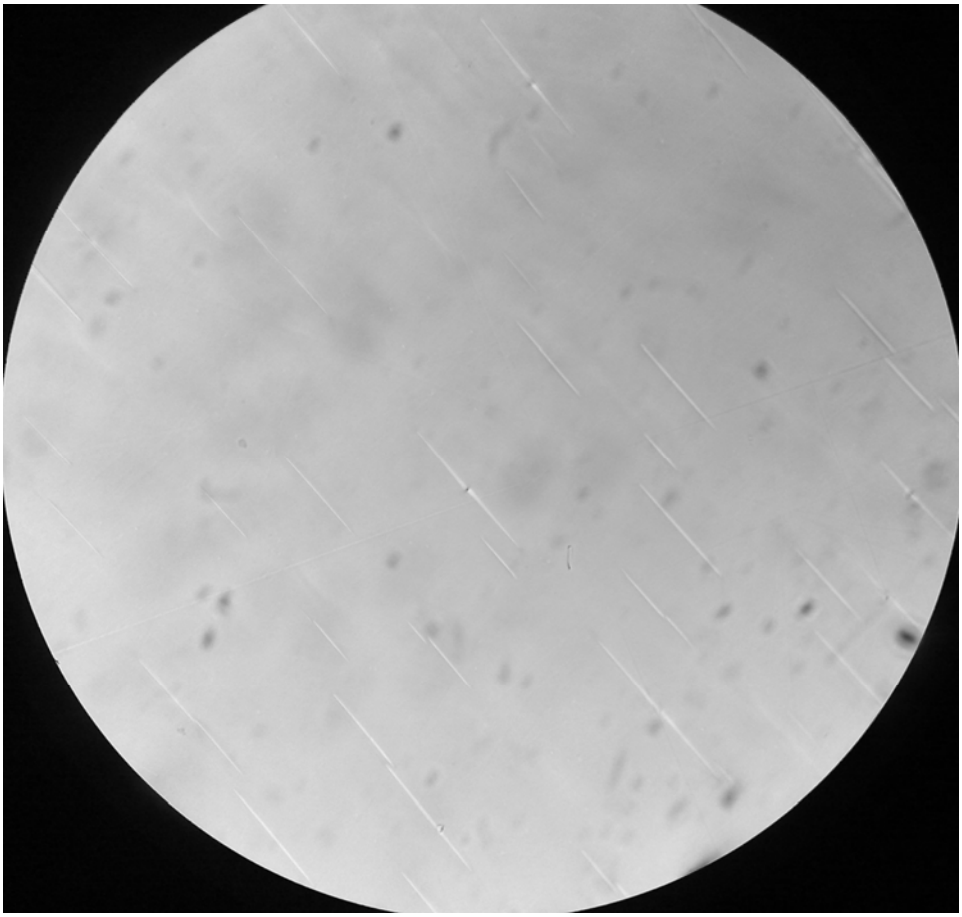

Figure 2

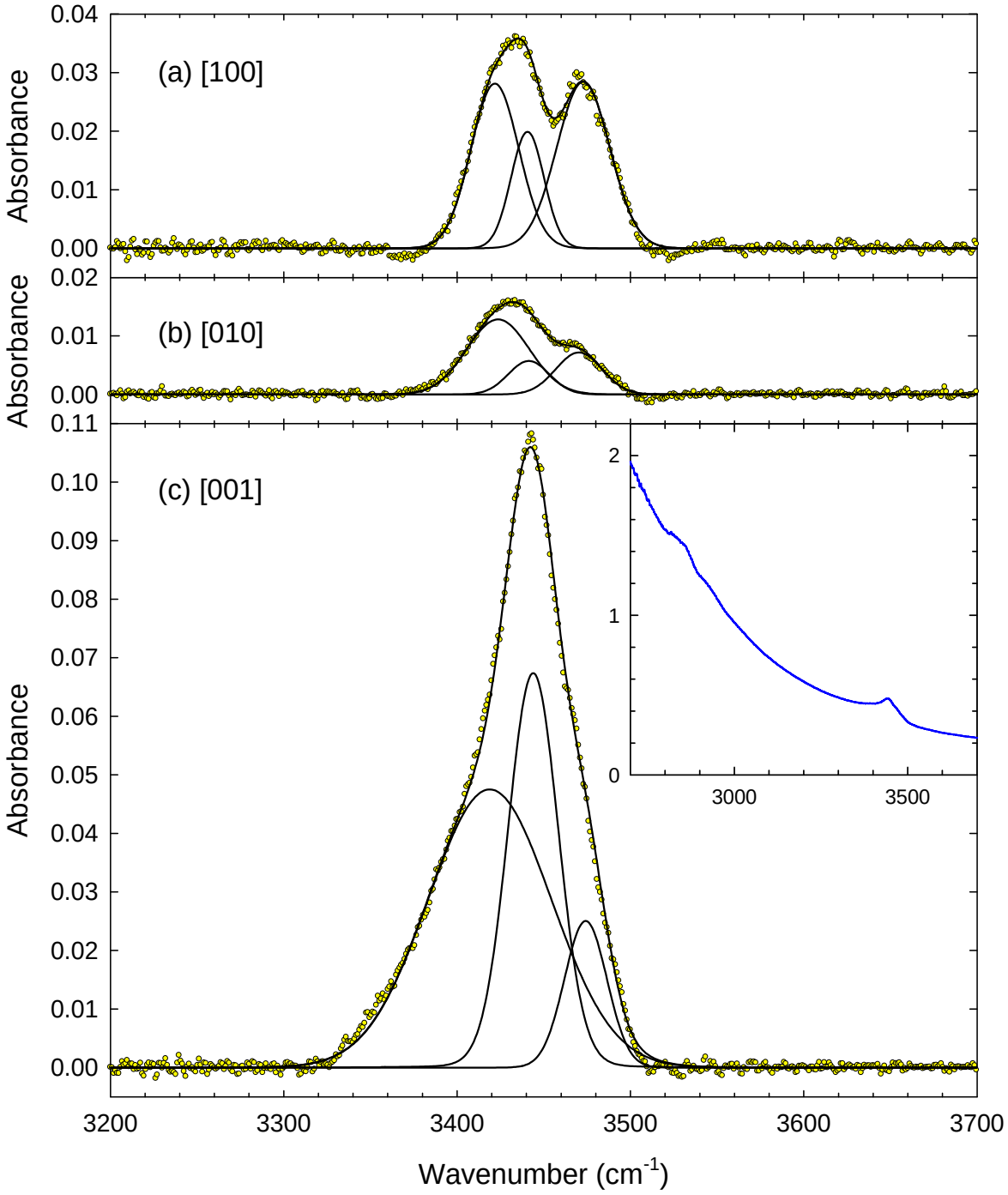
(a) [100]
(b) [010]
(c) [001]
Absorbance
Wavenumber (cm-1)
0.04
0.03
0.02
0.01
0.00
0.11
0.10
0.09
0.08
0.07
0.06
0.05
3200
3300
3400
3500
3600
3700
2
1
0
3000
3500

Figure 3

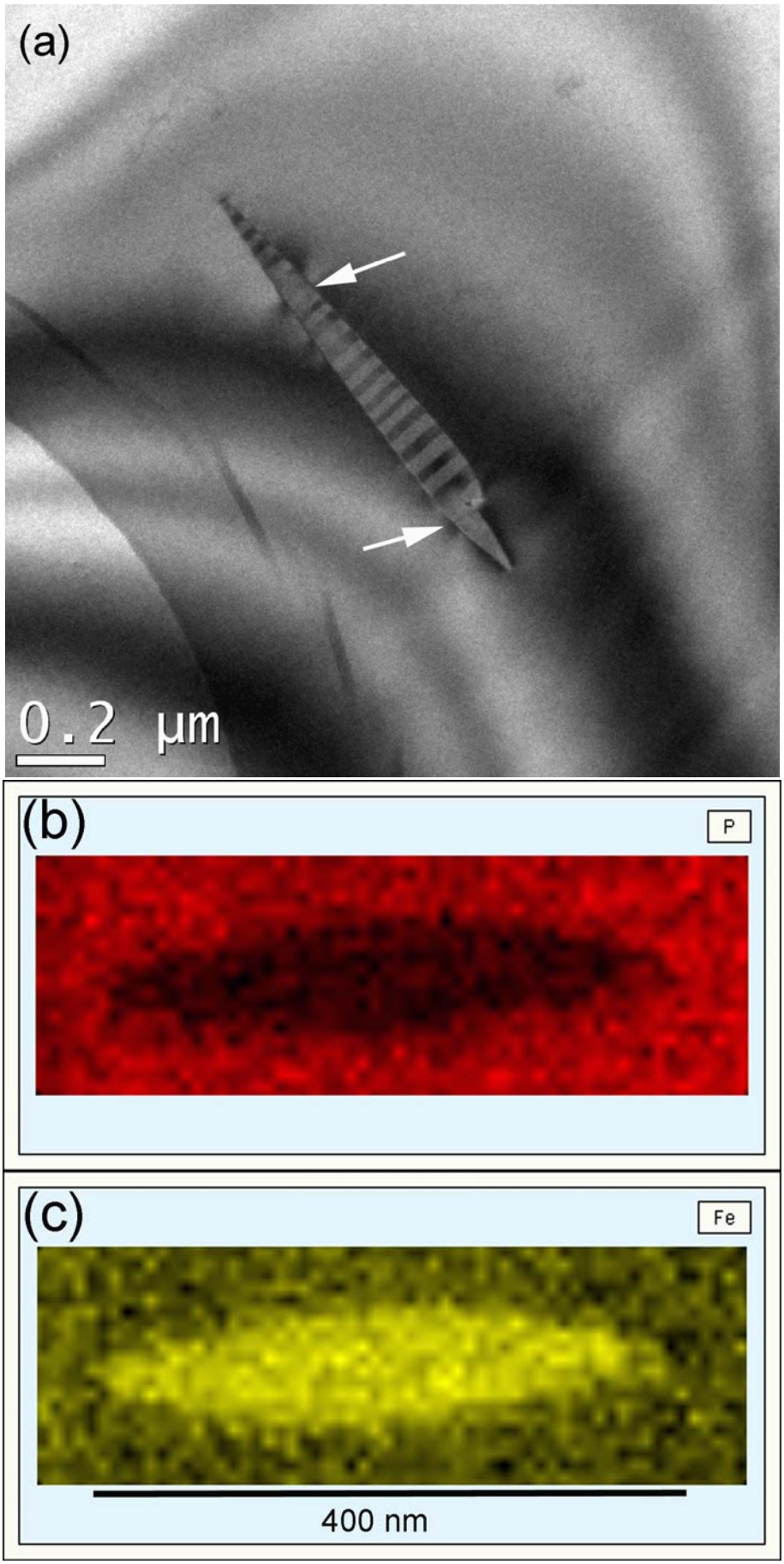

Figure 4

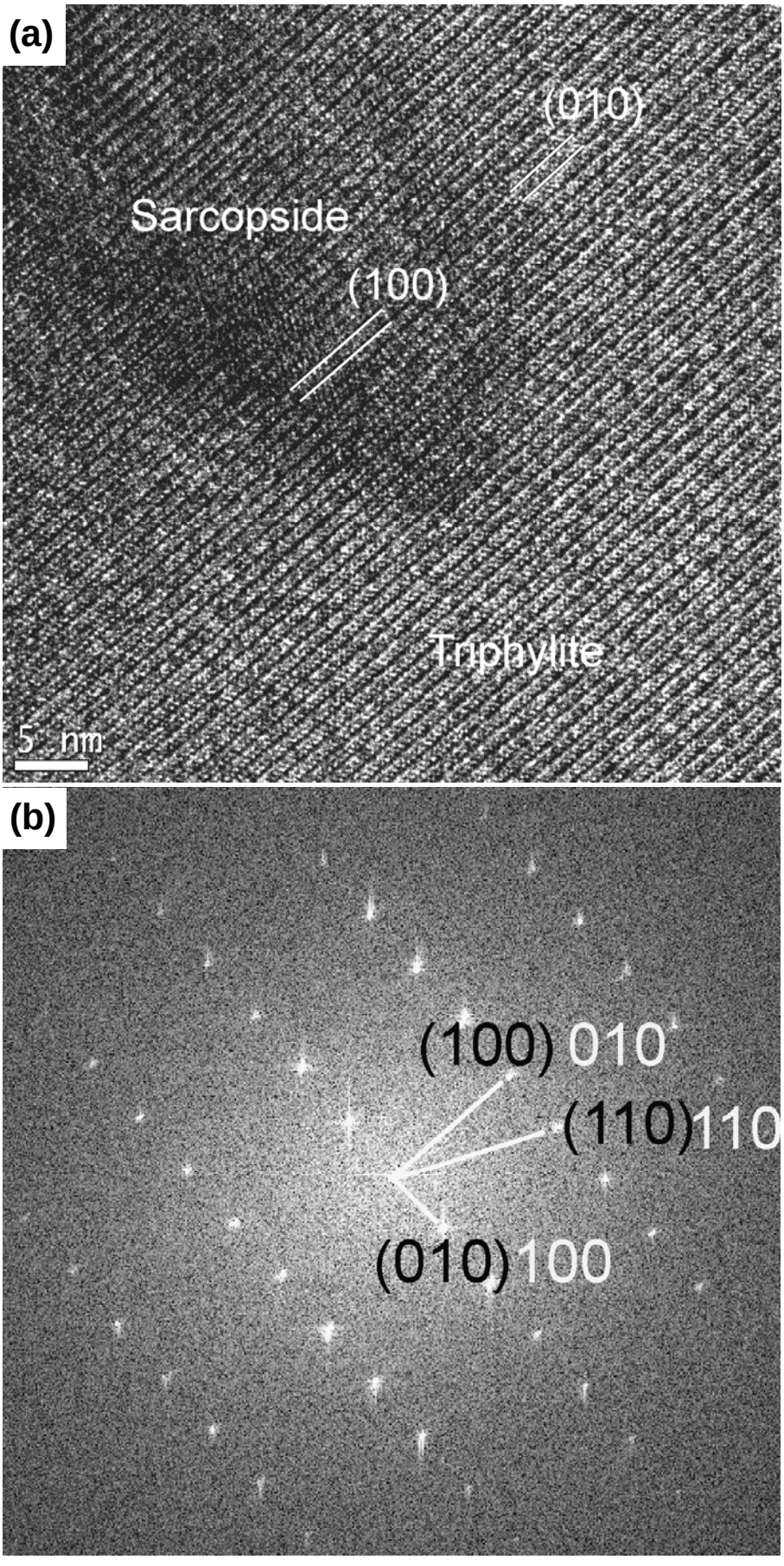

Figure 5

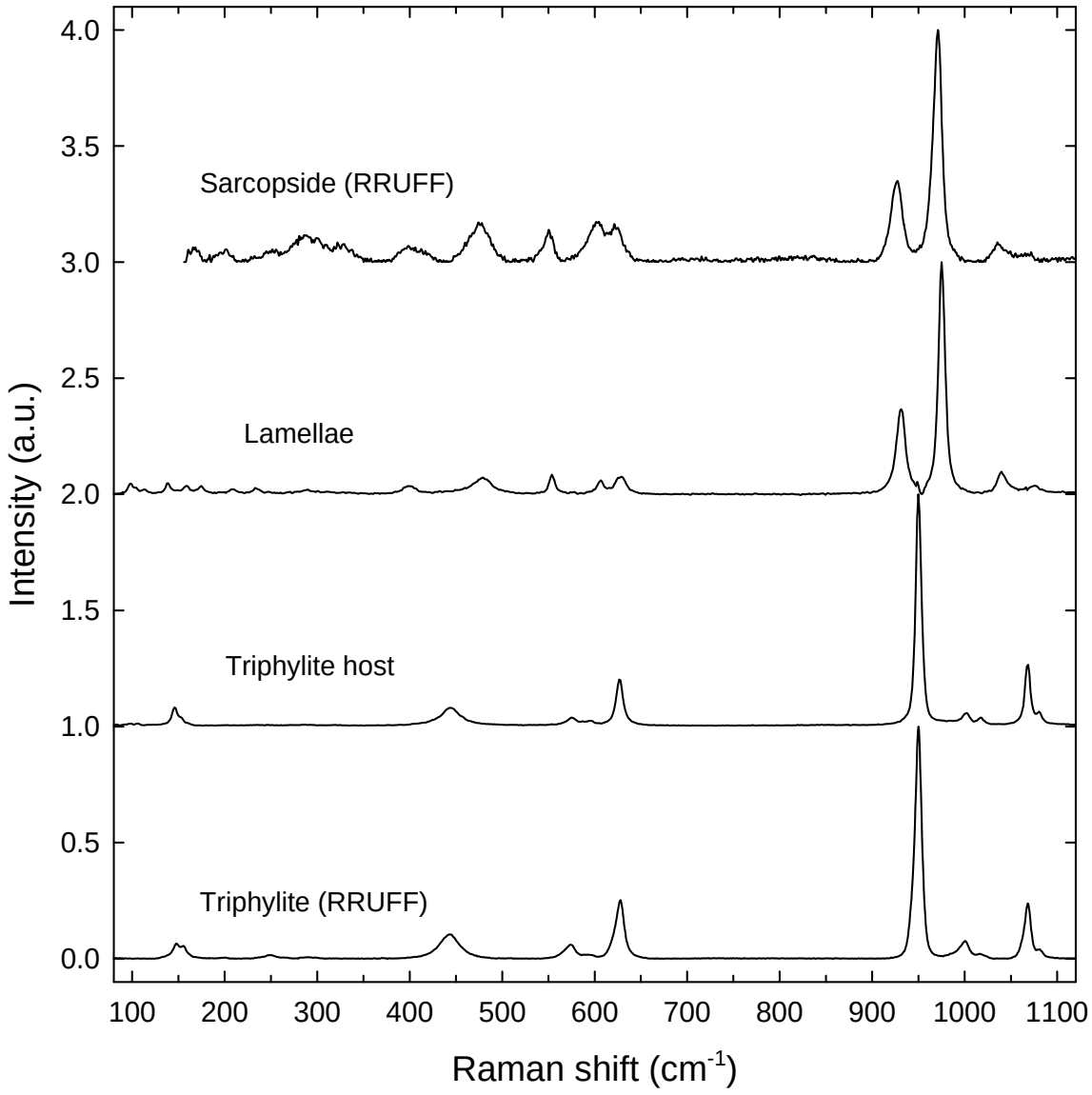
Sarcopside (RRUFF)
Lamellae
Triphylite host
Triphylite (RRUFF)
Intensity (a.u.)
Raman shift (cm-1)
4.0
3.5
3.0
2.5
2.0
1.5
1.0
0.5
0.0
100
200
300
400
500
600
700
800
900
1000
1100

Figure 6